Static dipole polarizability of alkali-metal clusters: Electronic exchange and correlation effects

A. Rubio and L. C. Balbás
Departamento de Física Teórica, Atómica y Nuclear, Universidad de Valladolid, E-47011 Valladolid, Spain

Ll. Serra and M. Barranco*
Departament de Física, Universitat de les Illes Balears, E-07071 Palma de Mallorca, Spain
(Received 19 July 1990)

Nonlocal approximations for the electronic exchange and correlation effects are used to compute, within density-functional theory, the polarizability and surface-plasma frequencies of small jellium-like alkali-metal clusters. The results are compared with those obtained using the local-density approximation and with available experimental data, showing the relevance of these effects in obtaining an accurate description of the surface response of metallic clusters.

I. INTRODUCTION

The characteristics of the surface response of metallic systems to an external field are related to the screening of the field from their interior. The recent experimental determination of some properties of small metallic clusters[1-6] has revealed the importance of quantum size effects for systems with a very high surface-to-volume ratio. To be specific, for small alkali-metal clusters containing a few tens of atoms, an enhancement of the polarizability[1] and a red shift of the surface-plasma resonance wavelength[2-6] have been observed with respect to the predicted classical values for a metallic sphere of identical size.[7]

The quantum study of metallic clusters usually assumes the spherical jellium model[8] (SJM) for the ionic positive charge and describes the valence electronic cloud by means of the density-functional theory[9] (DFT) within the local-density approximation[10] (LDA) for exchange and correlation (XC) effects. The response to external fields is then calculated within the framework of linear-response theory[11] by means of the time-dependent local-density approximation[12,13] (TDLDA). The polarizabilities of sodium neutral clusters calculated by this method[12] or, equivalently, by solving the so-called Sternheimer equation,[14] are higher than the classical predictions but are still about 20% lower than experiments. Similarly, TDLDA predictions of the surface resonance frequencies of small jelliumlike clusters[12,13] are correctly red shifted with respect to the classical Mie formula[7] but are still blue shifted with respect to experiments. Analogous conclusions are reached by using the random-phase-approximation (RPA) sum-rule approach in connection with the LDA description of jelliumlike metallic clusters.[15-17]

Despite the qualitative agreement of the LDA predictions with the experimental trends, the question remains what percent of the quantitative disagreement is due to the jellium model for the ionic charge and what percent is due to the LDA description of the electronic cloud. A recent calculation of the polarizabilities of jelliumlike alkali-metal clusters[18] is able to reduce by about one-half the discrepancy between the LDA results and experiments by including some self-interaction corrections into the LDA XC potential.[19] The LDA has been successfully applied to obtain the total energy in atoms, molecules, surfaces, and solids. However, for studying the surface response it is of great importance to have a good description of the electronic density tail and single-electron energy levels, both of them being well-known drawbacks of the LDA.[19]

In this work we go beyond the LDA by using the so-called weighted-density approximation (WDA) for exchange and correlation effects.[20,21] For spherically symmetric neutral clusters, the WDA XC potential tends to $-1/2r$ at large r, which is a substantial improvement over the exponential decay of the LDA XC potential. In order to reproduce the $-1/r$ asymptotic behavior of the exact XC potential, we will use a further approximation in the spirit of the WDA, which was first introduced by Przybylski and Borstel (PB).[22] This approximation, here called the "PB approximation," has been explored in previous works[23,24] for atoms and metallic clusters yielding very promising results. We will show in this paper that the PB XC potential leads to relevant improvements with respect to the LDA predictions for the polarizabilities and surface resonance frequencies of alkali-metal jellium-like clusters.

This paper is organized as follows. In Sec. II the different formalisms we will use to calculate the polarizability and surface collective frequencies are sketched. In Sec. II A a short explanation of the WDA and PB approximations to density-functional theory is given, and in Sec. II B we generalize the Sternheimer equation[14] to be used within the WDA and PB XC potentials. The external field-induced XC potential is related to the so-called "XC static local field correction" to the dielectric function, which shows radical differences for WDA or PB approximations as compared with the LDA one. Section II C contains a short account of the RPA sum-rule approach as previously used by some of us[15,16] to estimate the average energy of the surface collective frequencies of metallic clusters within the LDA. Here we generalize the sum rules to be used within the WDA or PB approxima-

tions. In Sec. III we present and discuss our results for the ground-state properties (Sec. III A), for the polarizabilities (Sec. III B), and for the surface collective frequencies (Sec. III C) of small alkali-metal clusters, and in Sec. IV we present the conclusions. Appendix A contains details on the deduction of the WDA induced potential and Appendix B provides an outline of the numerical procedures used in the calculation.

II. THEORY

A. The weighted-density approximation

In the spherical jellium model,[8] a metallic cluster is described by a homogeneous spherical background of positive charge (representing the ions) with density $n_+(\mathbf{r})=n_+^0$ for $r \le R$ (the sphere radius R depends on the number of atoms N), and a distribution of valence electrons (one per atom in the case of a neutral alkali-metal cluster), which is calculated self-consistently solving the Kohn-Sham (KS) equations of the density-functional formalism[9,10] (Hartree atomic units will be used unless explicitly indicated):

$$[-\tfrac{1}{2}\nabla^2+V_{\rm eff}(\mathbf{r})]\psi_i(\mathbf{r})=\varepsilon_i\psi_i(\mathbf{r}) \ . \tag{1}$$

The effective potential $V_{\rm eff}$ is the sum of the ionic (positive jellium), electron-electron (Hartree), and exchange-correlation contributions,

$$V_{\rm eff}(\mathbf{r})=V_{\rm jel}(\mathbf{r})+V_H(\mathbf{r})+V_{\rm XC}(\mathbf{r}) \ , \tag{2}$$

and the ground-state (g.s.) electron density $n(\mathbf{r})$ is evaluated from the occupied single-electron orbitals $\psi_i(\mathbf{r})$:

$$n(\mathbf{r})=\sum_{i=1}^{N}|\psi_i(\mathbf{r})|^2 \ . \tag{3}$$

$V_{\rm XC}(\mathbf{r})$ contains all the many-electron effects missing in V_H and is determined after some approximation is assumed for the exchange-correlation energy functional, $E_{\rm XC}[n]$, a key ingredient of the DFT.

In the usual LDA, $V_{\rm XC}(r)$ is determined by the local density $n(\mathbf{r})$ at point $\mathbf{r}$. Although there is ample evidence that LDA is accurate enough for many practical purposes in atomic, molecular, and solid-state calculations, nevertheless there are problems in which the LDA is not good enough.[19] A nonlocal WDA was proposed some years ago[20,21] aiming at removing some of the deficiencies of the LDA. The WDA has been applied by some of us[24] to the study of cluster fragmentation. We give here only a brief account of the most salient features of the WDA, referring the reader to our previous work[23] for more details.

In DFT, the electron exchange-correlation energy can be exactly expressed as[25]

$$E_{\rm XC}=\tfrac{1}{2}\int d\mathbf{r}\, n(\mathbf{r})\int d\mathbf{r}'\frac{n(\mathbf{r}')G(\mathbf{r},\mathbf{r}')}{|\mathbf{r}-\mathbf{r}'|} \ , \tag{4}$$

where $G(\mathbf{r},\mathbf{r}')$ is the pair-correlation function. The XC potential $V_{\rm XC}$ is obtained as the functional derivative of $E_{\rm XC}$:

$$V_{\rm XC}(\mathbf{r})\equiv\frac{\delta E_{\rm XC}}{\delta n(\mathbf{r})}=V_1(\mathbf{r})+V_2(\mathbf{r})+V_3(\mathbf{r}) \tag{5}$$

with

$$V_1(\mathbf{r})=\tfrac{1}{2}\int\frac{n(\mathbf{r}')}{|\mathbf{r}-\mathbf{r}'|}G(\mathbf{r},\mathbf{r}')d\mathbf{r}' \ , \tag{5a}$$

$$V_2(\mathbf{r})=\tfrac{1}{2}\int\frac{n(\mathbf{r}')}{|\mathbf{r}-\mathbf{r}'|}G(\mathbf{r}',\mathbf{r})d\mathbf{r}' \ , \tag{5b}$$

$$V_3(\mathbf{r})=\tfrac{1}{2}\int\int\frac{n(\mathbf{r}')n(\mathbf{r}'')}{|\mathbf{r}'-\mathbf{r}''|}\frac{\delta G(\mathbf{r}',\mathbf{r}'')}{\delta n(\mathbf{r})}d\mathbf{r}'\,d\mathbf{r}'' \ . \tag{5c}$$

The WDA makes the *ansatz*

$$G(\mathbf{r},\mathbf{r}')=G^{\rm WDA}(|\mathbf{r}-\mathbf{r}'|;\bar{n}(\mathbf{r})) \ , \tag{6}$$

where $G^{\rm WDA}(|\mathbf{r}-\mathbf{r}'|;\bar{n}(\mathbf{r}))$ is the pair-correlation function of a homogeneous electron gas of constant density equal to $\bar{n}(\mathbf{r})$, which is determined at each point $\mathbf{r}$ by requiring the normalization of the exchange-correlation hole for one electron at $\mathbf{r}$,

$$\int d\mathbf{r}'\, n(\mathbf{r}')G^{\rm WDA}(|\mathbf{r}-\mathbf{r}'|;\bar{n}(\mathbf{r}))=-1 \ . \tag{7}$$

For the pair-correlation function we use the expression derived by Chacon and Tarazona,[26] which is given in a convenient analytical form.

The exact pair-correlation function has the symmetry property $G(\mathbf{r},\mathbf{r}')=G(\mathbf{r}',\mathbf{r})$. This leads to $V_1(\mathbf{r})=V_2(\mathbf{r})$ and then

$$V_{\rm XC}(\mathbf{r})=2V_1(\mathbf{r})+V_3(\mathbf{r}) \ . \tag{8}$$

For a neutral atom or finite cluster the asymptotic behavior of $V_{\rm XC}$ is then[19] $-1/r$. However, $G^{\rm WDA}$ is nonsymmetric due to the dependence on $\bar{n}(\mathbf{r})$. The consequence is that for the WDA XC potential

$$V_{\rm XC}^{\rm WDA}(\mathbf{r})=V_1^{\rm WDA}(\mathbf{r})+V_2^{\rm WDA}(\mathbf{r})+V_3^{\rm WDA}(\mathbf{r}) \tag{9}$$

we have $V_1^{\rm WDA}(\mathbf{r})\neq V_2^{\rm WDA}(\mathbf{r})$ and then[21] $V_{\rm XC}^{\rm WDA}(\mathbf{r})\approx -1/2r$. This is a significant improvement over the LDA, in which $V_{\rm XC}^{\rm LDA}(\mathbf{r})$ decays exponentially at large r, but the spurious $\frac{1}{2}$ factor that appears in the WDA still leads to some difficulties, as pointed out in Ref. 23. A way to remedy this situation was explored in previous papers.[23,24] It consists of forcing the behavior of $V_{\rm XC}(\mathbf{r})$ embodied in Eq. (8) and thus the correct asymptotic behavior. Using this procedure, proposed by Przybylski and Borstel,[22] the exchange-correlation potential is written as

$$V_{\rm XC}^{\rm PB}(\mathbf{r})=2V_1^{\rm WDA}(\mathbf{r})+V_3^{\rm WDA}(\mathbf{r}) \ . \tag{10}$$

The price paid for the improvement in $V_{\rm XC}^{\rm WDA}$ is that $V_{\rm XC}^{\rm PB}$ is not the functional derivative of $E_{\rm XC}^{\rm WDA}$ but the functional derivative of some unknown $E_{\rm XC}^{\rm PB}$. Consequently, one cannot in principle evaluate the exchange-correlation energy. However, in Ref. 23 we obtained good XC and total energies by evaluating $E_{\rm XC}^{\rm WDA}[n]$ employing the $n^{\rm PB}$ density. For the purposes of the present work, we do not need to evaluate total energies. Rather, it is important to have a good g.s. electronic density profile and the corresponding structure of single-particle levels together with

the functional derivative of V_{XC} with respect to the density. So the use of V_{XC}^{PB} will be consistent throughout this paper irrespective of the fact that we do not know the E_{XC}^{PB} functional leading to V_{XC}^{PB}.

In the case of the LDA, $E_{XC}[n]$ is expressed as

$$E_{XC}^{LDA}[n]=\int n\varepsilon_{XC}^{LDA}(n)d\mathbf{r} , \tag{11}$$

where $\varepsilon_{XC}^{LDA}(n)$ is the XC energy density per electron of the homogeneous electron gas of density $n(\mathbf{r})$. Evidently, the LDA needs no explicit knowledge of the pair-correlation function $G(\mathbf{r},\mathbf{r}')$. In our LDA calculations we express ε_{XC} as a sum of exchange and correlation contributions:

$$\varepsilon_{XC}\equiv\varepsilon_X+\varepsilon_C=-\frac{3}{4}\left[\frac{3}{\pi}\right]^{1/3}n^{1/3} -0.44\left[7.8+\left[\frac{3}{4\pi n}\right]^{1/3}\right]^{-1} , \tag{12}$$

where the first and the second term on the right-hand side are, respectively, the Dirac (exchange) and Wigner (correlation) energy densities per particle of the homogeneous electron gas at density n.[25] From Eqs. (11) and (12), the LDA XC potential is easily obtained as

$$V_{XC}^{LDA}(r)\equiv\frac{\delta E_{XC}^{LDA}}{\delta n}=\varepsilon_{XC}(n)+n\frac{\partial\varepsilon_{XC}}{\partial n} . \tag{13}$$

B. The Sternheimer equation

To obtain the electronic multipolar polarizability of alkali-metal clusters, we will solve self-consistently the modified Sternheimer equation as used first by Mahan[27] for atoms and later by Beck[14] for clusters. Here we generalize the equations to be used within the WDA and PB approximations. We will deal with alkali-metal clusters whose g.s. properties are obtained solving the Kohn-Sham (KS) equations (1)–(3) within the SJM, and restrict ourselves to spherically symmetric clusters, i.e., clusters with closed electronic shells.

When an external multipole potential of the form

$$\delta V_L(\mathbf{r})=r^L Y_L^0(\hat{\mathbf{r}}) \tag{14}$$

is acting on one of these clusters, the g.s. orbitals ψ_i, and the g.s. density $n(\mathbf{r})$ are changed to first order to $\psi_i+\delta\psi_i$ and $n(\mathbf{r})+\delta n(\mathbf{r})$, respectively. The induced electronic charge $\delta n(\mathbf{r})$ is

$$\delta n(\mathbf{r})=4\mathrm{Re}\sum_i \psi_i^*(\mathbf{r})\delta\psi_i(\mathbf{r}) , \tag{15}$$

where the sum runs over all occupied orbitals. Here, i designates the usual quantum numbers $i\equiv(n,l,m)$, and Eq. (15) includes a factor 2 due to the spin degeneracy. The Lth-order polarizability is computed from the induced density as

$$\alpha_L=\frac{4\pi}{2L+1}\int d\mathbf{r}\, r^L Y_L^0(\hat{\mathbf{r}})\delta n(\mathbf{r}) . \tag{16}$$

First-order perturbation theory is used to obtain $\delta\psi_i$ and $\delta n(\mathbf{r})$, which leads to the Sternheimer equations[14,27]

$$[-\tfrac{1}{2}\nabla^2+V_{\mathrm{eff}}(\mathbf{r})-\varepsilon_i]\delta\psi_i(\mathbf{r})=-\delta V_{\mathrm{eff}}(\mathbf{r})\psi_i(\mathbf{r}) , \tag{17}$$

where V_{eff} is given by Eq. (2) and

$$\delta V_{\mathrm{eff}}(\mathbf{r})=r^L Y_L^0(\hat{\mathbf{r}})+\delta V_H(\mathbf{r})+\delta V_{XC}(\mathbf{r}) \tag{18}$$

is the induced potential made of the external potential $r^L Y_L^0(\hat{\mathbf{r}})$, the induced Hartree potential

$$\delta V_H(\mathbf{r})=\int d\mathbf{r}'\frac{\delta n(\mathbf{r}')}{|\mathbf{r}-\mathbf{r}'|} , \tag{19}$$

and the induced XC potential

$$\delta V_{XC}(\mathbf{r})=\int d\mathbf{r}'\frac{\delta V_{XC}(\mathbf{r})}{\delta n(\mathbf{r}')}\delta n(\mathbf{r}') . \tag{20}$$

The functional derivative in this last term

$$\frac{\delta V_{XC}(\mathbf{r})}{\delta n(\mathbf{r}')}=\frac{\delta^2 E_{XC}[n]}{\delta n(\mathbf{r})\delta n(\mathbf{r}')} , \tag{21}$$

which represents the so-called "XC static local field correction" to the dielectric function, is evaluated at the unperturbed g.s. density $n(\mathbf{r})$. For spherically symmetric g.s. densities, it is possible to reduce Eqs. (17) and (18) to radial equations. This can be seen by solving iteratively these equations as follows. Taking $\delta n^{(0)}=0$ as a first approximation leads to a first $\delta V_{\mathrm{eff}}^{(1)}(\mathbf{r})=r^L Y_L^0(\hat{\mathbf{r}})\equiv\delta V_{\mathrm{eff},L}^{(1)}(r)Y_L^0(\hat{\mathbf{r}})$, and due to the assumed shell closure, one obtains from Eqs. (17) and (15) a first-induced density $\delta n^{(1)}(\mathbf{r})=\delta n_L^{(1)}(r)Y_L^0(\hat{\mathbf{r}})$, having the same symmetry as the perturbing potential. This process will be continued until self-consistency if we are able to prove the following.

Lemma. For spherically symmetric electron systems, the substitution of

$$\delta n(\mathbf{r})=\delta n_L(r)Y_L^0(\hat{\mathbf{r}}) \tag{22}$$

into Eq. (18) leads to

$$\delta V_{\mathrm{eff}}(\mathbf{r})=\delta V_{\mathrm{eff},L}(r)Y_L^0(\hat{\mathbf{r}}) . \tag{23}$$

That is, the only nonzero terms in the expansion of $\delta n(\mathbf{r})$ and $\delta V_{\mathrm{eff}}(\mathbf{r})$ in spherical harmonics are those with the same symmetry as the perturbing potential $\delta V_L(\mathbf{r})$. Mahan[27] proved this lemma explicitly for the LDA case. We give here a proof for a general $V_{XC}(\mathbf{r})$. Substituting into Eq. (20) the induced density Eq. (22) and using the formal expansion

$$\frac{\delta V_{XC}(\mathbf{r})}{\delta n(\mathbf{r}')}=\sum_{l,m}\left[\frac{\delta V_{XC}(\mathbf{r})}{\delta n(\mathbf{r}')}\right]_{l,m}[Y_l^m(\hat{\mathbf{r}}')]^* Y_l^m(\hat{\mathbf{r}}) , \tag{24}$$

we obtain, due to the orthogonality property of the spherical harmonics,

$$\delta V_{XC}(\mathbf{r})=\delta V_{XC,L}(r)Y_L^0(\hat{\mathbf{r}}) \tag{25}$$

with

$$\delta V_{XC,L}(r)=\int dr'(r')^2\left[\frac{\delta V_{XC}(\mathbf{r})}{\delta n(\mathbf{r}')}\right]_{L,0}\delta n_L(r') . \tag{26}$$

A similar proof can be given for the induced Hartree potential, $\delta V_H(\mathbf{r})$, by using the well-known expansion of $|\mathbf{r}-\mathbf{r}'|^{-1}$ into spherical harmonics, resulting in

$$\delta V_H(\mathbf{r})=\delta V_{H,L}(r)Y_L^0(\hat{\mathbf{r}}) \tag{27}$$

with

$$\delta V_{H,L}(r)=\frac{4\pi}{2L+1}\int dr'(r')^2\frac{r_<^L}{r_>^{L+1}}\delta n_L(r') , \tag{28}$$

where $r_>$ ($r_<$) is the greater (smaller) of r and r'. Equations (25) and (28) complete the proof of the lemma.

In the LDA case, the radial component of the induced XC potential, $\delta V_{XC,L}^{LDA}(r)$, is easily obtained because the second functional derivative of E_{XC}^{LDA} in Eq. (21) is a diagonal matrix in the $\mathbf{r},\mathbf{r}'$ coordinates:

$$\frac{\delta V_{XC}^{LDA}(\mathbf{r})}{\delta n(\mathbf{r}')}=\frac{\delta^2 E_{XC}^{LDA}}{\delta n(\mathbf{r})\delta n(\mathbf{r}')}=\frac{\partial^2(n\varepsilon_{XC}^{LDA})}{\partial n^2}\delta(\mathbf{r}-\mathbf{r}') \tag{29}$$

leading to

$$\delta V_{XC,L}^{LDA}(r)=\frac{\partial^2(n\varepsilon_{XC}^{LDA})}{\partial n^2}\delta n_L(r) , \tag{30}$$

which is readily evaluated from Eq. (12). However, the XC static local field correction to the dielectric function, $\delta^2 E_{XC}/\delta n(\mathbf{r})\delta n(\mathbf{r}')$, is a symmetric nondiagonal matrix in the case of the WDA, whereas $\delta V_{XC}^{PB}(\mathbf{r})/\delta n(\mathbf{r}')$ leads to a nonsymmetric matrix in the $\mathbf{r},\mathbf{r}'$ coordinates. Correspondingly, the WDA and PB explicit expressions of $\delta V_{XC,L}(r)$ are more involved than the LDA ones. Within the WDA defined by Eqs. (6) and (7) one gets for $\delta V_{XC,L}(r)$,

$$\delta V_{XC,L}^{WDA}(r)=\delta V_{1,L}^{WDA}(r)+\delta V_{2,L}^{WDA}(r)+\delta V_{3,L}^{WDA}(r) . \tag{31}$$

The explicit expression of each term in Eq. (31) is given in Appendix A. For the PB XC potential, one obtains

$$\delta V_{XC,L}^{PB}(r)=2\delta V_{1,L}^{WDA}(r)+\delta V_{3,L}^{WDA}(r) , \tag{32}$$

where $\delta V_{1,L}^{WDA}$ and $\delta V_{3,L}^{WDA}$ are the same as in Eq. (31) but evaluated now at the n^{PB} g.s. density.

Using Eqs. (22) and (23) it is possible to reduce Eqs. (17) and (18) to radial equations. Writing

$$\psi_i(\mathbf{r})=\frac{u_{nl}(r)}{r}Y_l^m(\hat{\mathbf{r}}) , \tag{33}$$

$$\delta\psi_i(\mathbf{r})=\sum_{l',m'}\frac{f_{l'm'}^i(r)}{r}Y_{l'}^{m'}(\hat{\mathbf{r}}) , \tag{34}$$

[recall that i means (n,l)] and projecting Eq. (17) onto $Y_{l_1}^{m_1}(\hat{\mathbf{r}})$, we obtain, after angular integration,

$$\left[-\frac{1}{2}\frac{d^2}{dr^2}+\frac{l_1(l_1+1)}{2r^2}+V_{eff}(r)-\varepsilon_{nl}\right]f_{l_1m_1}^i(r) = -a(m;L,l,l_1)\delta V_{eff,L}(r)u_{nl}(r) , \tag{35}$$

where the coefficient

$$a(m;L,l,l_1)=\int d\hat{\mathbf{r}}\, Y_L^0 Y_l^m Y_{l_1}^{m_l *} \tag{36}$$

is nonzero only if $m_1=m$. Multiplying both sides of Eq. (35) by $a(m;L,l,l_1)$ and summing for all m values, we obtain

$$\left[-\frac{1}{2}\frac{d^2}{dr^2}+\frac{l_1(l_1+1)}{2r^2}+V_{eff}(r)-\varepsilon_{nl}\right]v_{l_1,L}^i(r) = -\delta V_{eff,L}(r)u_{nl}(r) , \tag{37}$$

where

$$v_{l_1,L}^i(r)=\frac{\sum_m a(m;L,l,l_1)f_{l_1m}^i(r)}{A(L,l,l_1)} \tag{38}$$

and

$$A(L,l,l_1)=\sum_m a^2(m;L,l,l_1) . \tag{39}$$

The radial induced density can be expressed now as

$$\delta n_L(r)=4\,\mathrm{Re}\sum_{n,l,l'}\frac{u_{nl}^*(r)v_{l'L}^i}{r^2}A(L,l,l') . \tag{40}$$

For the case of interest in this work, i.e., the dipole polarizability, we have $L=1$, and it is easy to show that

$$A(1,k,k')=(1/4\pi)[(k+1)\delta_{k',k+1}+k\delta_{k',k-1}] , \tag{41}$$

which reduces to two the number of coupled equations (37) and (40) to be solved for each unperturbed orbital i. We have obtained $\delta n_L(r)$ for the LDA, WDA, and PB approximations using standard matrix methods after discretizing the radial distance, imposing the boundary conditions $\delta n(\infty)=0$ and $\delta n(0)=0$, the latter one in order to have $\delta n(\mathbf{r})$ well defined at $r=0$. In Appendix B some details are given about the numerical procedure.

C. RPA sum-rule approach within the WDA

The RPA sum-rule approach has been used recently to study the multipole surface modes of metallic clusters.[15,16] Here we only sketch the main features of the method, referring the reader to our previous papers[15,16,28] and references therein for more details.

From the moments m_k of the strength function $S(E)$,

$$m_k=\int E^k S(E)dE=\sum_\rho \varepsilon_\rho^k|\langle\rho|Q|\psi\rangle|^2 , \tag{42}$$

where Q is the external field acting on the system, and ε_ρ, $|\rho\rangle$, and $|\psi\rangle$ are the excitation energies, excited states, and the g.s. of the system, respectively, one can obtain the average energy $\bar{E}$ and variance σ^2 of the strength as $\bar{E}=m_1/m_0$ and $\sigma^2=m_2/m_0-(m_1/m_0)^2$, respectively. Defining $E_k\equiv(m_k/m_{k-2})^{1/2}$, it has been shown that

$$E_1\le\bar{E}\le E_3 , \tag{43}$$

$$\sigma^2\le\tfrac{1}{4}(E_3^2-E_1^2) . \tag{44}$$

Consequently, one may estimate the centroid and variance of $S(E)$ by evaluating the three RPA moments m_{-1}, m_1, and m_3. Odd $S(E)$ moments can be obtained with RPA precision as expectation values of suitable commutators on the KS ground state $|\psi\rangle$. For m_1 and m_3 we have

$$m_1=\tfrac{1}{2}\langle\psi|[Q,[H,Q]]|\psi\rangle\ , \tag{45}$$

$$m_3=\tfrac{1}{2}\langle\psi|[[H,[H,Q]],[H,Q]]|\psi\rangle\ . \tag{46}$$

m_{-1} is given by the polarizability α of the system as

$$m_{-1}=\tfrac{1}{2}\alpha\ . \tag{47}$$

We will consider here the operator $Q=r^L Y_L^0$, which generates surface oscillations. A direct evaluation of m_1 yields[15] (in this section we write $\hbar$, m, and e explicitly)

$$m_1=\frac{\hbar^2}{2m}L(2L+1)\int_0^\infty dr\, r^{2L}n(r)\ , \tag{48}$$

where $n(r)$ is the KS unperturbed g.s. equilibrium density. For $L=1$, m_1 is proportional to the electron number, and in this case the three approximations we are discussing yield the same result. In Ref. 15 the explicit expressions of the m_3 contributions are given corresponding to the kinetic energy density $m_3(T)$, the Hartree Coulomb energy $m_3(H)$, and the jellium-electron (JE) Coulomb energy m_3(JE). $m_3(T)$ can be written as

$$m_3(T)=\left[\frac{\hbar^2}{m}\right]L(2L+1)(L-1)\times\int_0^\infty dr\frac{\hbar^2}{2m}r^{2L-2}[L\tau(r)+\tfrac{1}{2}(L-2)\lambda(r)]\ , \tag{49}$$

where $\tau(r)=\sum_i|\nabla\psi_i|^2$ is the electron kinetic energy density and the function $\lambda(r)$ represents a centrifugal kinetic-energy density

$$\lambda(r)=\frac{1}{4\pi r^2}\sum_{n,l}2(2l+1)l(l+1)\frac{|u_{nl}|^2}{r^2}\ , \tag{50}$$

where $u_{nl}(r)/r$ is the radial single-electron wave function.

The Coulombic terms $m_3(H)$ and m_3(JE) are (see Ref. 15 for a thorough discussion)

$$m_3(H)=-e^2\left[\frac{\hbar^2}{m}\right]^2L^2(L-1)\times\int_0^\infty dr\, n(r)r^{2L-3}\int_0^r d\mathbf{r}'\, n(r') \tag{51}$$

and

$$m_3(\mathrm{JE})=2\pi e^2\left[\frac{\hbar^2}{m}\right]^2L^2\times\int_0^\infty dr\, r^{(2L-2)}n'(r)\int_0^r dr'\,(r')^2 n_{\mathrm{jel}}(r')\ , \tag{52}$$

where $n'(r)$ is the density derivative with respect to r, and n_{jel} is the constant jellium density $n_{\mathrm{jel}}(r)=n_+^0\theta(R-r)$.

The $m_3(T)$, $m_3(H)$, and m_3(JE) expressions are the same for the LDA, WDA, and PB approximations. The numerical values differ only because the g.s. densities are different in the three cases. It is worth noting that for $L=1$, the only nonzero contribution to m_3 is the jellium-electron one, Eq. (52), which is the only translational symmetry-breaking term in the energy density functional.[15]

For operators Q such that $\Delta Q=0$, there is no contribution to m_3 from the XC energy term within the LDA (see Sec. II B of Ref. 28). Due to the WDA and PB *Ansätzes*, m_3(XC) is not rigorously zero. To illustrate this point we start with a series expansion of the scaled XC energy functional:

$$E_{\mathrm{XC}}[n_\eta]=E_{\mathrm{XC}}[n]+\int\frac{\delta E_{\mathrm{XC}}}{\delta n}\delta n(\mathbf{r})d\mathbf{r}+\tfrac{1}{2}\int\frac{\delta^2E_{\mathrm{XC}}}{\delta n(\mathbf{r})\delta n(\mathbf{r}')}\delta n(\mathbf{r})\delta n(\mathbf{r}')d\mathbf{r}\,d\mathbf{r}'+\cdots\ , \tag{53}$$

where

$$\delta n(\mathbf{r})\equiv n_\eta-n=\eta n_1+\eta^2n_2+\cdots\ . \tag{54}$$

We can now write the XC contribution to m_3 as (only quadratic terms in η^2 are needed)

$$m_3(\mathrm{XC})=\int\frac{\delta E_{\mathrm{XC}}}{\delta n}n_2(\mathbf{r})d\mathbf{r}+\tfrac{1}{2}\int\frac{\delta^2E_{\mathrm{XC}}}{\delta n(\mathbf{r})\delta n(\mathbf{r}')}n_1(\mathbf{r})n_1(\mathbf{r}')d\mathbf{r}\,d\mathbf{r}'\ . \tag{55}$$

In these expressions the functional derivatives must be evaluated at the g.s. density n.

For multipole operators of the form $Q_L=r^LY_L^0$ and for spherically symmetric systems, it is easy to obtain[15] for n_1 and n_2 of Eq. (54)

$$n_1(\mathbf{r})=-\frac{\hbar^2}{m}n'(r)Lr^{L-1}Y_L^0\ , \tag{56}$$

$$\int n_2(r)d\hat{\mathbf{r}}=\frac{\hbar^4}{2m^2}L^2r^{2L-3}[rn''(r)+2Ln'(r)]\ , \tag{57}$$

where n',n'' denotes the first and second density derivatives with respect to r. Finally, Eq. (55) can be written as

$$m_3(\mathrm{XC})=\frac{\hbar^4}{2m^2}L^2\int n'(r)\left[-r^{2L}\frac{dV_{\mathrm{XC}}}{dr}+r^{L+1}\int n'(r')r'^{L+1}\delta^2E_{\mathrm{XC},L}\,dr'\right]dr\ , \tag{58}$$

where

$$\delta^2E_{\mathrm{XC},L}=\int\frac{\delta^2E_{\mathrm{XC}}}{\delta n(\mathbf{r})\delta n(\mathbf{r}')}Y_L^0(\hat{\mathbf{r}})Y_L^0(\hat{\mathbf{r}}')d\hat{\mathbf{r}}\,d\hat{\mathbf{r}}'\ . \tag{59}$$

It is also possible from Eq. (58) to obtain $m_3(H)$ substituting E_{XC}, V_{XC}, and $\delta^2E_{\mathrm{XC},L}$ by E_H, V_H, and $\delta^2E_{H,L}$, respectively.

For the case $L=1$ one should expect a null m_3(XC) due to the translational symmetry. We have checked that its value for the clusters we have studied is very small,

which provides a posterior test on the consistency of the approximations we have used.

III. RESULTS AND DISCUSSION

A. Ground-state properties of alkali-metal clusters

We have self-consistently solved the KS Eqs. (1)–(3) for spherical Na_N ($N=8$, 18, 20, 34, 40, 58, and 92) neutral clusters, as well as for the Na^+_{N+1}, K^+_{N+1}, Na^-_{N-1}, K^-_{N-1} ($N=8$, 20, and 40) charged ones, using the WDA, PB, and LDA XC potentials of Eqs. (9), (10), and (13), respectively. The Coulomb potential created by the jellium is

$$V_{\rm jel}(\mathbf{r})=\begin{cases}\frac{2\pi}{3}n_+^0 r-2\pi R^2 n_+^0, & r\le R\\ -\frac{N}{R}=-\left[\frac{4\pi}{3}\right]R^3 n_+^0/r, & r\ge R\ ,\end{cases}\tag{60}$$

where the radius R of the cluster is related to the number of atoms N by the equality $\frac{4}{3}\pi R^3=N\Omega$, Ω being the volume per atom, which is assumed for simplicity to be the same as in the bulk metal. For alkali metals, with one valence electron per atom, we have $\Omega=\frac{4}{3}\pi r_s^3$, r_s being the radius per valence electron. In this work we use $r_s=4$

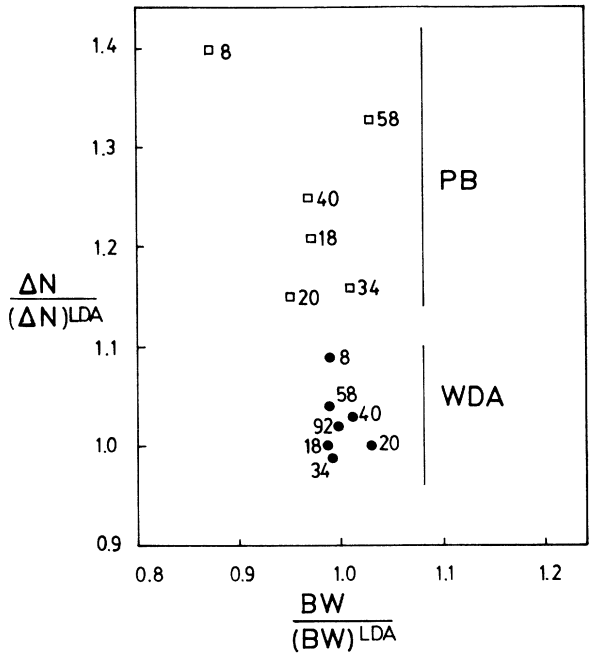

FIG. 2. Spill out (ΔN) and bandwidth (BW) of the spherical Na_N cluster for the WDA (dots) and PB (squares) calculations in units of the corresponding LDA values. The number of atoms in the cluster is also shown.

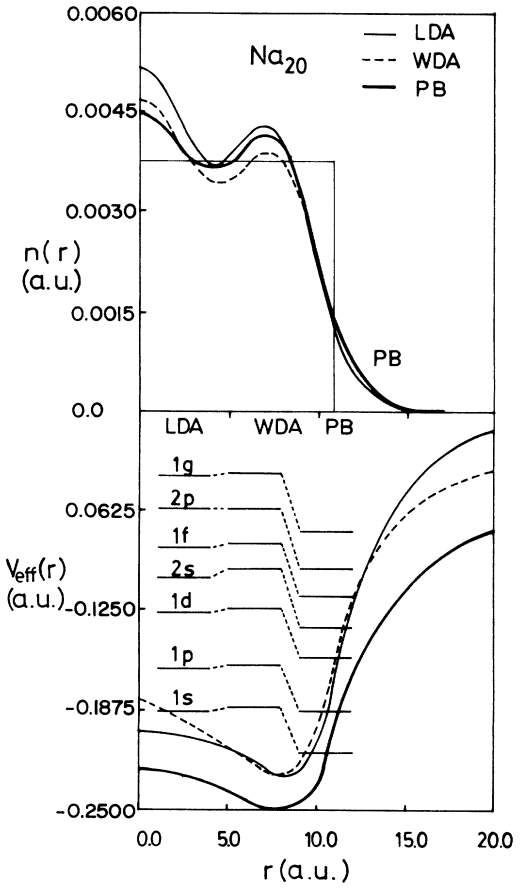

FIG. 1. Electron densities, eigenvalues, and effective potentials for the Na_{20} cluster obtained by self-consistently solving the Kohn-Sham equations within the LDA (thin lines), WDA (dashed lines), and PB (thick lines) approximations for exchange-correlation effects. Also shown is the jellium constant density n_+^0.

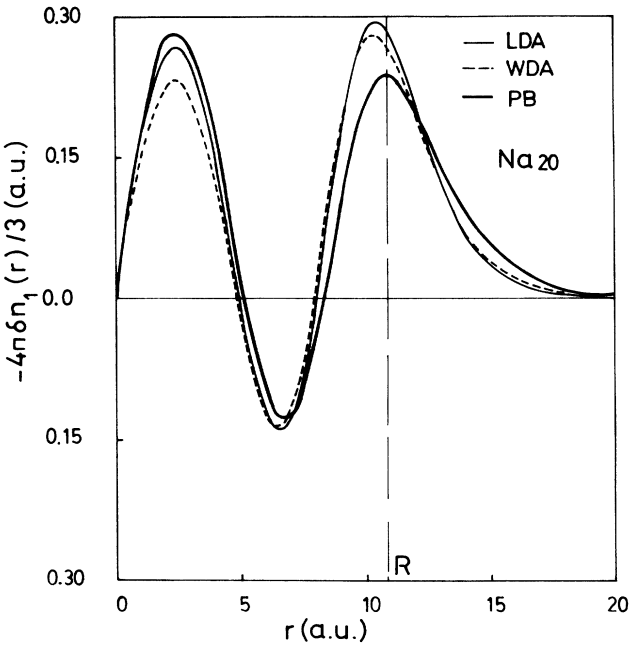

FIG. 3. Na_{20} induced densities δn_1 corresponding to LDA (thin line), WDA (dashed line), and PB (thick line) calculations. The vertical line shows the jellium radius.

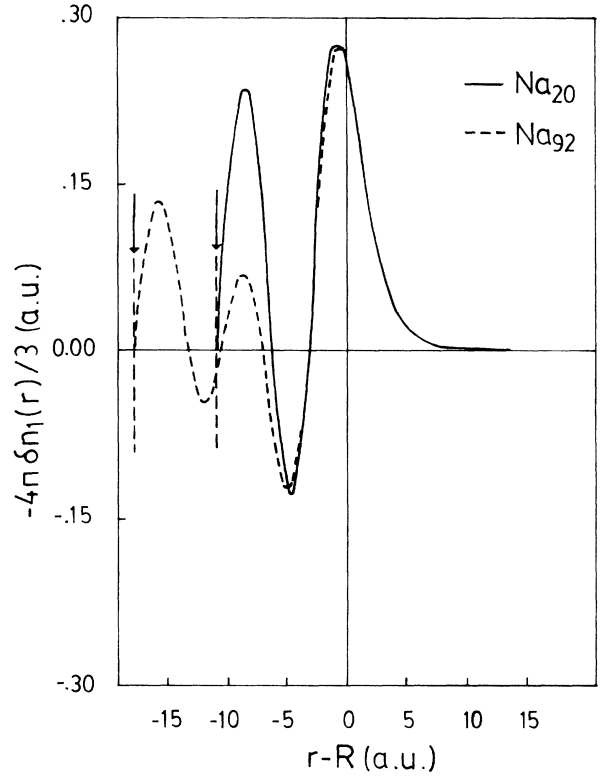

FIG. 4. Na_{20} and Na_{92} induced densities δn_1^{WDA}. The origin is fixed at the jellium edge of each cluster. The arrows indicate the center of the clusters.

TABLE I. Calculated dipole polarizabilities of neutral Na_N and K_N clusters within the LDA, WDA, and PB approximations for exchange-correlation effects. WDA/PB refers to the calculation of α_1 using the induced density $\delta^{WDA}(n^{PB})_1$ (see Sec. III B). The unit is $\alpha_{Cl}=R^3$, with $R=r_s N^{1/3}$. (For Na, $r_s=4$ a.u., and for K, $r_s=4.86$ a.u.). The experimental values are extracted from Ref. 4.

			Na		
N	LDA	WDA	PB	WDA/PB	Expt.
8	1.45	1.49	1.64	1.81	1.72
18	1.33	1.37	1.47	1.59	1.63
20	1.37	1.42	1.51	1.63	1.62
34	1.27	1.30	1.37	1.47	1.57
40	1.32	1.37	1.44	1.53	1.57
58	1.22	1.25	1.31	1.39	
			K		
N	LDA	WDA	PB	WDA/PB	
8	1.32	1.38	1.52	1.68	
20	1.28	1.33	1.41	1.52	

a.u. for sodium and $r_s=4.86$ a.u. for potassium.

Figure 1 shows for the neutral Na_{20} cluster the KS densities, effective potentials, and electron single-particle levels ($2s$ in this case is the highest occupied orbital) corresponding to the LDA (thin lines), WDA (dashed lines), and PB (thick lines) approximations. Also shown is the jellium constant density n_+^0. Note in Fig. 1 the different density tails and effective potentials for the three cases, n^{PB}, extending to a larger distance than the other densi-

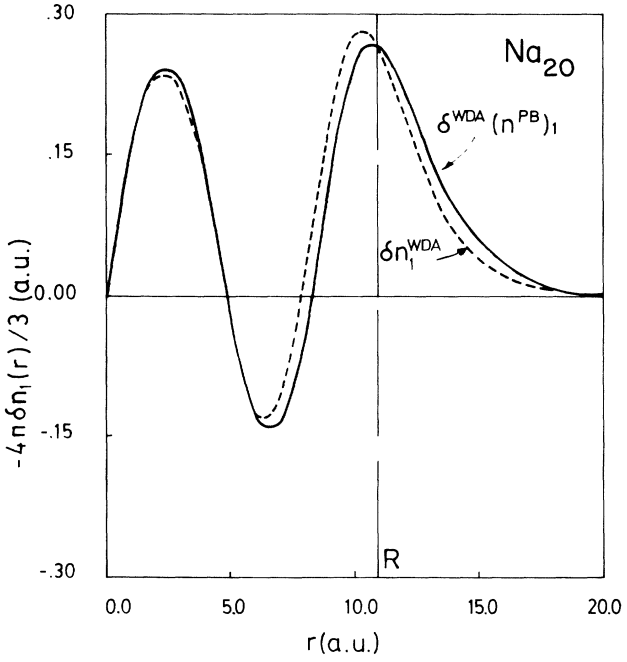

FIG. 5. Comparison of the induced densities δn_1^{WDA} (dashed line) and $\delta^{WDA}(n^{PB})_1$ (solid line) for the Na_{20} cluster.

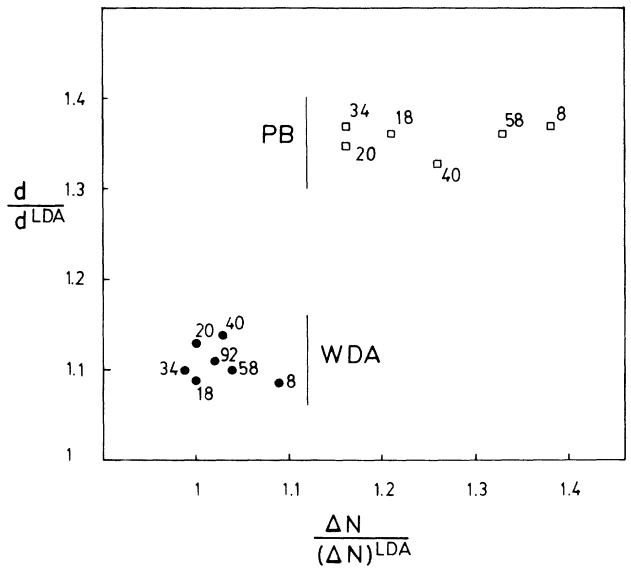

FIG. 6. The centroid of the WDA induced charge density (dots) and PB (squares) calculations in units of the corresponding LDA values vs the spill-out parameter (also in units of the corresponding LDA values) for spherical Na_N clusters. The number of atoms in the cluster is also shown.

ties. A quantitative measurement of this fact is furnished by the amount of electronic charge beyond the jellium edge (electronic spill out)

$$\Delta N = \int_R^\infty n(r) d\mathbf{r} \ . \tag{61}$$

We note that the oscillation in the WDA and PB electron densities near the jellium edge is depressed as compared to the LDA one. A similar fact has been obtained recently for planar surfaces in calculations beyond the LDA.[29,30]

Also noticeable is the different magnitude of the eigenvalues obtained in the three approximations. In exact DFT, the absolute value of the eigenvalue of the last occupied orbital, $|\varepsilon_{\rm HO}|$, coincides with the exact ionization potential of the system, whereas the eigenvalues of the remaining orbitals cannot be interpreted as one-electron removal energies.[19] In a previous paper,[31] we presented evidence suggesting that for atoms, $V_{\rm XC}^{\rm PB}$ leads to $|\varepsilon_{\rm HO}|$ in good agreement with atomic ionization potentials. Even more, the remaining occupied orbitals have eigenvalues that are in good agreement with experimental removal energies. By contrast, $|\varepsilon_{\rm HO}^{\rm LDA}|$ severely underestimates the ionization potential.[19] The same facts have also been found for alkali-metal clusters.[32–34] The different average level spacing given by LDA, WDA, and PB calculations can be quantified by the width of the occupied band (BW), defined as the energy difference between the highest and lowest occupied levels. Since the level spacing and the electron density tail are important for the response of the clusters to external fields, we plot in Fig. 2 the spill out [see Eq. (61)], and the bandwidth for the WDA and PB calculations relative to the corresponding LDA values. Only values for closed-shell configurations are plotted corresponding to $N=8$ ($1p$), 18 ($1d$), 20 ($2s$), 34 ($1f$), 40 ($2p$), 58 ($1g$), and 92 ($3s$) electrons (magic numbers). For the PB case, $N=92$ is not a magic number because the usual orbital sequence $1g,2d,1h,3s$ is changed to $1g,2d,1h,1i,2g,3s$. For the WDA calculation neither the spill out nor the BW change substantially with respect to the LDA values. [For a planar jelliumlike surface the calculated[35] ($\Delta N^{\rm WDA}/\Delta N^{\rm LDA}$) ratio is 1.039 for sodium ($r_s=4$), increasing to 1.073 for $r_s=6$, and decreasing to 1.014 for $r_s=2$.] However, the PB calculation yields about a 20% ΔN increase and about a 6% BW decrease (except for Na_{34} and Na_{58}) with respect to the corresponding LDA results. The importance of these changes on the surface response will be shown in the next sections.

B. Polarizabilities of neutral and charged alkali-metal clusters

We have obtained the dipolar $L=1$ induced densities $\delta n_1(r)$ of alkali-metal clusters, corresponding to the LDA, WDA, and PB approximations by self-consistently solving the Sternheimer equations. A check on the overall accuracy of the numerical procedures (see Appendix B) is provided by the Sorbello electrostatic force sum rule,[36] which states that the electrostatic potential due to the external field and the induced charge distribution should vanish at the surface of the jellium sphere, leading to

$$\frac{4\pi}{3}\left[\frac{1}{R^3}\int_0^R dr\, r^3 \delta n_1(r) + \int_R^\infty \delta r\, dn_1(r)\right] = -\frac{N_-}{N_+} \ , \tag{62}$$

where N_+ (N_-) is the total positive (negative) charge. For the calculations reported here, Eq. (62) is satisfied within $\pm 0.1\%$ for the LDA and WDA cases, and $\pm 0.2\%$ for the PB calculation.

Figure 3 shows $\delta n_1^{\rm LDA}(r)$ (thin line), $\delta n_1^{\rm WDA}(r)$ (dashed line), and $\delta n_1^{\rm PB}(r)$ (thick line) for the Na_{20} neutral cluster, and Fig. 4 shows $\delta n_1^{\rm WDA}(r)$ for the Na_{20} and Na_{92} clusters. As noted by Ekardt[12] and Beck[14] in their LDA calculations, the hump at the jellium sphere radius looks very similar to $\delta n_1(r)$ for a planar jellium surface calculated within the LDA.[37] Moreover, this hump depends very little on the cluster size, as illustrated in Fig. 4. Notice from Fig. 3 that the maximum of $\delta n_1(r)$ at the surface is, in the WDA and PB cases, smaller than in the LDA case. This is due to the different electronic structure and the different XC-induced potential [see Fig. 1 and the comments below Eq. (61)]. Inside the cluster, the amplitude of the induced density reflects the amount of charge available to screen the external field. This amplitude is reduced as the size of the cluster increases (see Fig. 4), converging towards the planar surface result as seen by Beck.[14] The different response inside the cluster of $\delta n_1^{\rm LDA}$, $\delta n_1^{\rm WDA}$, and $\delta n_1^{\rm PB}$ shown in Fig. 3 reflects not only the different charge density but also the different structure of the "XC static local field correction" to the

TABLE II. Calculated dipole polarizabilities of positively (N^+) and negatively (N^-) charged alkali-metal clusters in units of $\alpha_{\rm Cl}=R^3$. $N^{+/-}$ refers to a cluster with N atoms and $N-1$ electrons (+) or ($N+1$) electrons (−). LDA, WDA, PB, and WDA/PB correspond to the different approximations for exchange-correlation effects (See Sec. III B).

	K				Na			
$N^{+/-}$	LDA	WDA	PB	WDA/PB	LDA	WDA	PB	WDA/PB
9^+	1.18	1.21	1.28	1.42	1.24	1.27	1.35	1.48
21^+	1.19	1.23	1.28	1.38	1.25	1.29	1.35	1.44
41^+	1.19	1.23	1.28	1.35	1.25	1.28	1.34	1.42
7^-	1.73	1.94	2.28	2.55	1.98	2.24	2.60	2.88
19^-	1.43	1.56	1.69	1.83	1.57	1.72	1.85	1.99
39^-	1.32	1.41	1.50	1.60	1.43	1.53	1.62	1.72

dielectric function, $\delta^2 E_{XC}/\delta n(\mathbf{r})\delta n(\mathbf{r}')$. To gain further insight into this fact, we have plotted in Fig. 5 for the Na_{20} the induced densities δn_1^{WDA} and $\delta^{WDA}(n^{PB})_1$, the latter one obtained using in the Sternheimer Eqs. (37)–(40), the $\delta V_{XC,1}^{WDA}(r)$ of Eq. (31), and self-consistently solving these equations using the g.s. u_{nl}^{PB} orbitals and ε_{nl}^{PB} eigenvalues. In other words, the induced potential $\delta V_{XC,1}^{WDA}(\mathbf{r})$ and the corresponding induced density $\delta^{WDA}(n^{PB})_1$ are calculated starting from the unperturbed $n^{PB}(\mathbf{r})$ density. We see in Fig. 5 that $\delta^{WDA}(n^{PB})_1$ inside the cluster is similar to δn_1^{WDA} and not to the δn_1^{PB} shown in Fig. 3, whereas outside the cluster $\delta^{WDA}(n^{PB})_1$ is similar to δn_1^{PB}. This means that inside the cluster, the response depends mainly on the structure of the screening given by the XC local field correction, whereas outside the cluster it mainly depends on the electronic density tail. The XC local field correction, $\delta^2 E_{XC}/\delta n(\mathbf{r})\delta n(\mathbf{r}')$, should be a symmetric matrix in the $\mathbf{r},\mathbf{r}'$ coordinates, and this is so for the WDA, whereas we obtain a nonsymmetric matrix for the PB case, as we pointed out in Sec. II B. Based on this fact, we consider the induced density $\delta^{WDA}(n^{PB})_1$ to be more realistic than the δn_1^{PB} one. The same prescription was adopted in Ref. (23) to evaluate the atomic XC energies by using $E^{WDA}[n^{PB}]$, leading to good results. Of course, the results presented below based on $\delta^{WDA}(n^{PB})_1$ should be taken with some caution, since the calculation is no longer fully self-consistent.

From the calculated $\delta n_1(r)$ we obtain the cluster polarizability by means of Eq. (16). The LDA, WDA, and PB neutral sodium cluster polarizabilities are compared to experiments[4] in Table I. The polarizabilities obtained from $\delta^{WDA}(n^{PB})_1$ are also included under the heading WDA/PB. The units are the classical polarizability[7] $\alpha_{Cl}=R^3$ for a metallic sphere of radius R. The WDA does not improve the LDA predictions substantially, whereas the PB and WDA/PB calculations reduce the average 20% discrepancy of LDA with experiments to about 8% and 5%, respectively, on the average. The origin of the small WDA improvement is the better description of the screening inside the clusters. Actually, outside the cluster there are no significant differences between δn_1^{WDA} and δn_1^{LDA} (see Fig. 3). On the contrary, the improvement of the PB predictions with respect to the LDA ones is mainly due to the better description of the external part of $\delta n_1(r)$ (electronic spill out), whereas the WDA/PB calculations benefit from both WDA and PB improvements. These conclusions can be further supported by the results shown in Fig. 2 and Table I. We see in Fig. 2 that the g.s. properties relevant for the polarizability, namely the spill out and the bandwidth, are very similar for the WDA and LDA cases. Consequently, the systematic enhancement (about 3%) of the WDA polarizabilities with respect to the LDA ones is mainly due to the WDA structure of the XC local field correction in the Sternheimer equations. On the contrary, we see in Fig. 2 that ΔN^{PB} is 15–40 % larger than ΔN^{LDA}. This fact is the origin of the enhancement of α_1^{PB} with respect to α_1^{LDA}.

To gain deeper insight into the influence of the spill out on the polarizability, we have represented in Fig. 6 the parameter

$$d=\alpha_1^{1/3}-R \tag{63}$$

versus ΔN for the WDA and PB calculations in units of the corresponding LDA values. In the limit $R\to\infty$ the parameter d coincides[38] with the centroid of the induced electron density for a flat surface d_p, also called the image plane position. For the LDA case, d_p was calculated by Lang and Kohn,[37] who obtained $d_p^{LDA}=1.3\pm0.2$ for Na. Our calculated d^{LDA} values from Eq. (63) corresponding to Na_N clusters oscillate between 1.05 for $N=8$ and 1.21 for $N=198$, slowly converging towards d_p^{LDA} from below. In Fig. 6 we see that the calculated d^{WDA} values are about 9–14 % larger than the d^{LDA} ones for spill-out ratios in a range $0.9<\Delta N^{WDA}/\Delta N^{LDA}<1.09$, which

TABLE III. Calculated RPA E_1 and E_3 energies and variances, σ_M (in eV), of the dipole surface collective mode for Na_8 and Na_{20} neutral clusters compared to experimental surface-plasma resonance energies and widths from Ref. 4. LDA, WDA, PB, and WDA/PB refer to different approximations for the electronic exchange-correlation effects. Calculated values for the positively charged clusters Na_9^+ and Na_{21}^+ are also given.

	Na_8			Na_{20}		
	E_1	E_3	σ_M	E_1	E_3	σ_M
LDA	2.83	3.14	0.68	2.91	3.14	0.59
WDA	2.79	3.06	0.63	2.85	3.13	0.65
PB	2.65	2.95	0.65	2.77	3.06	0.65
WDA/PB	2.53	2.81	0.61	2.67	2.97	0.65
Expt.		$E=2.53$, $\Gamma=0.38$			$E=2.46$, $\Gamma=0.37$	
	Na_9^+			Na_{21}^+		
	E_1	E_3	σ_M	E_1	E_3	σ_M
LDA	3.05	3.16	0.41	3.04	3.19	0.48
WDA	3.02	3.16	0.46	2.94	3.18	0.61
PB	2.93	3.08	0.47	2.87	3.12	0.61
WDA/PB	2.79	2.93	0.45	2.77	3.03	0.61

means that the increase of d^{WDA} over d^{LDA} can be attributed mainly to the WDA XC local-field-correction improvement. In contradistinction, the calculated d^{PB} lie in a narrow band around 35% above the d^{LDA} value for a rather broad range of spill-out ratios $1.15 < \Delta N^{PB}/\Delta N^{LDA} < 1.38$. Taking these increments as valid in the limit $R \to \infty$, we would have $d_p^{WDA}/d_p^{LDA} \approx 1.1$ and $d_p^{PB}/d_p^{LDA} \approx 1.35$ for a sodium jellium surface. In a recent work,[29] Zhang *et al.* pointed out that the use of a nonlocal XC potential of the Langreth-Mehl type[39] would lead to a d_p bigger than the LDA one. However, a WDA surface calculation by Ossicini *et al.*[40] using a different pair-correlation function $G(r,r')$ than ours, leads to a d_p^{WDA} smaller than d_p^{LDA}. The authors of Ref. 40 also obtained a density hump near the jellium edge that is enhanced with respect to the one found in the LDA, contrary to other surface calculations[29,30] beyond LDA and to our WDA calculations for finite clusters. The influence of the pair-correlation function $G(r,r')$ on the WDA d_p calculations has been discussed by Chacon and Tarazona.[26]

In Table II the polarizabilities of the positively and negatively charged clusters Na_{N+1}^+, K_{N+1}^+, Na_{N-1}^-, and K_{N-1}^- are given ($N=8$, 20, and 40). For positively charged clusters, the effective potential is deeper than for neutral clusters and the electronic response is reduced, whereas for negatively charged clusters the reduction of the potential-well depth allows the electronic density to penetrate further into the vacuum, thus increasing the polarizability.

We want to end this section with some remarks about the corrections to the SJM due to the real granularity of the ionic distribution. Equation (63) allows one to express the polarizability in a form based on the classical equation $\alpha_1 = R_{\text{eff}}^3$, where the effective radius $R_{\text{eff}} = R + d$ is the sum of the radius R of the ionic distribution plus an electronic contribution expressed by the polarizability parameter d. The radius R taken in the SJM is larger than the one obtained by model calculations that incorporate more-realistic ionic distributions (see, for example, Ref. 41 for Na_N clusters and Ref. 42 for Al_N clusters). The fact that the observed polarizability for Al_N clusters[43] in the range $N \leq 40$ is smaller than the one predicted by the SJM-LDA approximation has been explained in Ref. 42 using a model that leads to an ionic distribution radius smaller than the SJM one. For small sodium clusters, the same model does not yield such a reduction.[44] For flat surfaces, discrete-lattice corrections to the jellium model have been obtained,[29] resulting in an effective surface shifted inwards for the jellium edge for aluminum, whereas it is only slightly shifted outwards for sodium. We thus infer that discrete-lattice corrections would have only a very little effect on the SJM polarizabilities of sodium clusters.

C. Surface-plasma resonance frequencies

In Table III the RPA E_1 and E_3 energies of the dipolar surface collective mode for Na_8 and Na_{20} neutral clusters are given, calculated from the expressions given in Sec. II C. To obtain E_1 we have used the sum rules m_1 and m_{-1}. It is worth noting that this energy is currently used as a mean energy in the so-called "plasmon pole approximation."[45] The surface-plasma resonance energy, E, should verify $E_1 < E < E_3$, with a variance σ such that $\sigma^2 \leq \frac{1}{4}(E_3^2 - E_1^2) \equiv \sigma_M^2$. We shall take the value σ_M as an estimate of the variance, but one should keep in mind that it is an upper bound to it. If the strength is mainly concentrated in a narrow energy region around the surface resonance, σ can be used to estimate the resonance width provided a line shape is assumed. For a Gaussian, it is easy to show that the width at half height Γ is given by $\Gamma = 2\sigma(2\ln 2)^{1/2} \sim 2.35\sigma$.

We see in Table III that the WDA/PB approximation yields results closer to the experimental E than the other approximations. Also given in Table III are the E_1 and

TABLE IV. Calculated RPA E_1 and E_3 energies and variances, σ_M (in eV), of the $L=1$ surface collective mode for the K_9^+ and K_{21}^+ clusters compared to the experimental surface-plasma resonance energies and widths from Ref. 5. LDA, WDA, PB, and WDA/PB refer to different approximations for the electronic exchange-correlations effects. Calculated values for the neutral K_8 and K_{20} clusters are also given.

	K_8			K_{20}		
	E_1	E_3	σ_M	E_1	E_3	σ_M
LDA	2.21	2.32	0.35	2.25	2.37	0.37
WDA	2.16	2.32	0.42	2.20	2.37	0.44
PB	2.06	2.24	0.44	2.14	2.32	0.45
WDA/PB	1.96	2.12	0.40	2.06	2.24	0.44
	K_9^+			K_{21}^+		
	E_1	E_3	σ	E_1	E_3	σ
LDA	2.33	2.39	0.26	2.32	2.40	0.31
WDA	2.30	2.39	0.32	2.29	2.40	0.36
PB	2.24	2.33	0.32	2.24	2.35	0.36
WDA/PB	2.13	2.22	0.31	2.16	2.28	0.36
Expt.		$E=1.93$, $\Gamma=0.22$			$E=1.98$, $\Gamma=0.16$	

TABLE V. Calculated RPA m_1 and m_3 sum rules (in a.u.) for the neutral Na_{40} cluster and LDA, WDA, PB, and WDA/PB calculations. The different contributions to m_3 are also displayed.

	m_1	m_3 (Tot)	m_3 (T)	m_3 (H)	m_3 (JE)	m_3 (XC)
$L=1$						
LDA	4.775	6.525×10^{-2}			6.525×10^{-2}	
WDA	4.775	6.524×10^{-2}			6.505×10^{-2}	1.851×10^{-4}
PB	4.775	6.317×10^{-2}			6.301×10^{-2}	1.627×10^{-4}
WDA/PB	4.775	6.037×10^{-2}			6.301×10^{-2}	-2.647×10^{-3}
$L=2$						
LDA	1.874×10^{3}	29.580	4.009	−23.124	48.695	
WDA	1.881×10^{3}	28.294	3.981	−23.106	48.403	−0.984
PB	1.958×10^{3}	28.859	3.777	−22.620	48.239	−0.536
WDA/PB	1.958×10^{3}	26.462	3.777	−22.620	48.239	−2.934
$L=3$						
LDA	5.905×10^{5}	1.039×10^{4}	3.304×10^{3}	-1.145×10^{4}	2.156×10^{4}	
WDA	6.006×10^{5}	9.477×10^{3}	3.254×10^{3}	-1.450×10^{4}	2.146×10^{4}	-7.306×10^{2}
PB	6.587×10^{5}	1.027×10^{4}	3.177×10^{3}	-1.480×10^{4}	2.226×10^{4}	-3.623×10^{2}
WDA/PB	6.587×10^{5}	9.087×10^{3}	3.177×10^{3}	-1.480×10^{4}	2.226×10^{4}	-1.550×10^{3}

E_3 RPA values for the positively charged cluster Na_9^+ and Na_{21}^+. We observe that the variance σ_M is smaller for the charged cluster than for the corresponding neutral cluster. In Table IV the calculated E_1 and E_3 for K_9^+ and K_{21}^+ are given, which are compared with the experimental energies from Ref. 5. The same comments as for Table III apply. Also given in Table IV are the E_1 and E_3 calculated values for the K_8 and K_{20} neutral clusters. We have used σ_M to estimate Γ as $\Gamma_M \sim 2.35\sigma_M$. The values we have obtained are around four times larger than the experimental values, indicating a rather wide spread of the dipole strength.

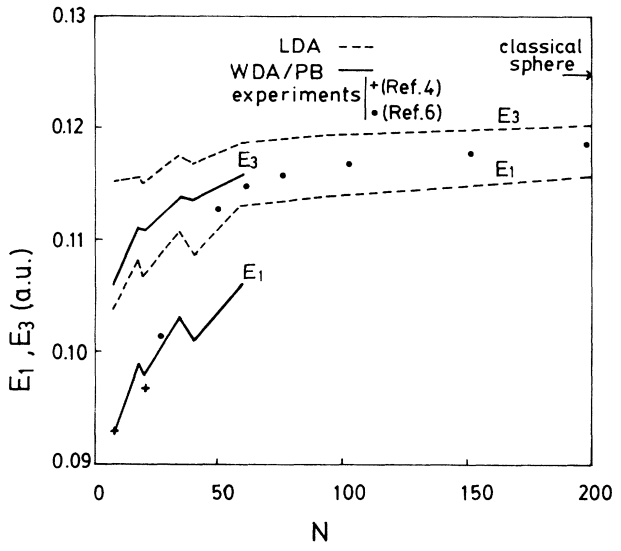

FIG. 7. RPA E_1 and E_3 energies of the $L=1$ mode for Na_N clusters vs N. Dashed lines correspond to LDA calculations and solid lines to WDA/PB calculations. Crosses and dots are experimental plasma resonance energies from Refs. 4 and 5, respectively.

In Fig. 7 the E_1 and E_3 energies of Na_N clusters calculated within the LDA and WDA/PB approximations are compared with some experimental plasma resonance energies from Refs. 4 and 6. The experimental values from Ref. 6 (dots in Fig. 7) correspond to the Na_N cluster adsorbed on a boron nitride surface and the number of atoms in the cluster, N, is actually an average value $\langle N \rangle$ around the size N. The experimental values for the Na_8 and Na_{20} clusters in Fig. 7 and Table III, and those for K_9^+ and K_{21}^+ correspond to free clusters. We see in Fig. 7 that our WDA/PB calculated E_1 and E_3 limits for the plasma resonance frequencies of small clusters follow quite well the experimental trend whereas the LDA ones fail for the smaller sizes.

In Table V are given the m_1 and m_3 sum rules for the Na_{40} $L=1$, 2, and 3 modes computed within the LDA, WDA, PB, and WDA/PB approximations. The different m_3 contributions are also displayed. For m_3 (XC), which is zero within the LDA for any L [see Ref. 28 or Eq. (58)], there is an explicit contribution within the nonlocal approximations used in this work. For the case $L=1$, one would still expect m_3 (XC)=0; therefore, the quoted $L=1$ values for m_3 (XC) in Table V corresponding to the nonlocal approximations set the limit of our numerical accuracy as well as of the consistency of these approximations in the present context.

IV. CONCLUSIONS

We have used the nonlocal WDA and related PB and WDA/PB approximations for the electronic exchange and correlation effects to study the dipole static polarizability of alkali-metal clusters. As compared with the LDA, these approximations yield a better description of the polarizability as a consequence, first, of a larger spill out of the g.s. electronic density, and second, of the

different structure of the induced V_{XC} potential.

It turns out that the first effect is more important in the case of the PB approximation than in the WDA, due to the better description of the asymptotic behavior of the V_{XC} achieved in the former approximation. Our calculations show that the second effect, which is taken into account in both the WDA and PB approximations, is better included in the WDA. Thus, the combination of the WDA "XC local field correction" with the PB g.s. density, here called the WDA/PB approximation, leads to a considerable improvement in the agreement between theory and experiment, decreasing the 20% average disagreement in LDA calculations to some 5% average disagreement in the WDA/PB case.

The equivalent for a cluster of the image plane distance d_p corresponding to a planar surface [see Eq. (63)] has been shown to be almost independent of the cluster size. In the PB case, the distance d for sodium is estimated to be some 35% larger than in the LDA.

We have also used the m_{-1}, m_1, and m_3 RPA sum rules to estimate the resonance mean energy in a plasmon pole approximation, i.e., making the hypothesis that the resonant state exhausts most of the dipole strength. We have also estimated an upper bound of the resonance width that has turned out to be rather gross.

Corrections to the SJM coming from discrete-ionic effects might have some effect on the polarizabilities. In the case of Na clusters, these effects will affect only slightly our calculated polarizabilities.

Finally, we would like to point out again the further approximation we have made to arrive at the weighted-density PB approximation (WDA/PB), whose use here is motivated by the circumstantial evidence that it yields the best results, not only for the polarizability of alkali-metal clusters, but also for the description of other atomic properties, such as single-electron eigenvalues, ionization potentials, and electron affinities.[31]

ACKNOWLEDGMENTS

We are indebted to Julio A. Alonso and to E. Chacon for useful discussions. This work has been supported by Júnta de Castilla Leon and Dirección General de Investigación Científica y Técnica (DGICYT) grants at the Universities of Valladolid, the Balearic Islands, and Barcelona.

APPENDIX A: RADIAL COMPONENTS OF THE WDA-INDUCED XC POTENTIAL

Here we obtain the explicit expression of each term in Eq. (31). For the $V_{XC}(\mathbf{r})$ [Eq. (5)] within the WDA *ansatz* for $G(\mathbf{r},\mathbf{r}')$ [Eqs. (6) and (7)], we have

$$\delta V_{XC}^{WDA}(\mathbf{r})=\delta V_1^{WDA}(\mathbf{r})+\delta V_2^{WDA}(\mathbf{r})+\delta V_3^{WDA}(\mathbf{r}) \tag{A1}$$

with

$$\delta V_1^{WDA}(\mathbf{r})=\tfrac{1}{2}\int \frac{\delta n(\mathbf{r}')}{|\mathbf{r}-\mathbf{r}'|}G^{WDA}(|\mathbf{r}-\mathbf{r}'|;\bar{n}(\mathbf{r}))d\mathbf{r}'+\tfrac{1}{2}\int \frac{n(\mathbf{r}')}{|\mathbf{r}-\mathbf{r}'|}d\mathbf{r}'\int \frac{\delta G^{WDA}(|\mathbf{r}-\mathbf{r}'|;\bar{n}(\mathbf{r}))}{\delta n(\mathbf{r}'')}\delta n(\mathbf{r}'')d\mathbf{r}'' , \tag{A2}$$

$$\delta V_2^{WDA}(\mathbf{r})=\tfrac{1}{2}\int \frac{\delta n(\mathbf{r}')}{|\mathbf{r}-\mathbf{r}'|}G^{WDA}(|\mathbf{r}-\mathbf{r}'|;\bar{n}(\mathbf{r}'))d\mathbf{r}'+\tfrac{1}{2}\int \frac{n(\mathbf{r}')}{|\mathbf{r}-\mathbf{r}'|}d\mathbf{r}'\int \frac{\delta G^{WDA}(|\mathbf{r}-\mathbf{r}'|;\bar{n}(\mathbf{r}'))}{\delta n(\mathbf{r}'')}\delta n(\mathbf{r}'')d\mathbf{r}'' , \tag{A3}$$

$$\delta V_3^{WDA}(\mathbf{r})=\int\int \frac{n(\mathbf{r}')}{|\mathbf{r}'-\mathbf{r}''|}\frac{\delta G^{WDA}(|\mathbf{r}'-\mathbf{r}''|;\bar{n}(\mathbf{r}'))}{\delta n(\mathbf{r})}\delta n(\mathbf{r}'')d\mathbf{r}'\,d\mathbf{r}''$$
$$+\tfrac{1}{2}\int\int \frac{n(\mathbf{r}')n(\mathbf{r}'')}{|\mathbf{r}'-\mathbf{r}''|}d\mathbf{r}'\,d\mathbf{r}''\int \frac{\delta^2 G^{WDA}(|\mathbf{r}'-\mathbf{r}''|;\bar{n}(\mathbf{r}'))}{\delta n(\mathbf{r})\delta n(\mathbf{r}_1)}\delta n(\mathbf{r}_1)d\mathbf{r}_1 . \tag{A4}$$

Expanding G^{WDA}, $\delta n(\mathbf{r}')$, and $|\mathbf{r}-\mathbf{r}'|^{-1}$ in spherical harmonics of the angle Ω between $\mathbf{r}$ and $\mathbf{r}'$,

$$G^{WDA}(|\mathbf{r}-\mathbf{r}'|;\bar{n}(\mathbf{r}))=\sum_p G_p(r,r')Y_p^0(\Omega) , \tag{A5}$$

$$\delta n(\mathbf{r}')\equiv\delta n_L(r')Y_L^0(\hat{\mathbf{r}}')$$
$$=\delta n_L(r')\sum_k\left[\frac{4\pi}{2L+1}\right]^{1/2}[Y_L^k(\Omega)]^*Y_L^k(\hat{\mathbf{r}}) , \tag{A6}$$

$$|\mathbf{r}-\mathbf{r}'|^{-1}=\sum_l\left[\frac{4\pi}{2l+1}\right]^{1/2}\frac{r_<^l}{r_>^{l+1}}Y_l^0(\Omega) , \tag{A7}$$

and taking the z axis along the $\mathbf{r}$ vector, the first integral in Eq. (A2) can be written as

$$\tfrac{1}{2}\int \frac{\delta n(\mathbf{r}')}{|\mathbf{r}-\mathbf{r}'|}G^{WDA}(|\mathbf{r}-\mathbf{r}'|;\bar{n}(\mathbf{r}))d\mathbf{r}'=\left[\tfrac{1}{2}\sum_{p,l}\frac{4\pi c(p,l,L)}{[(2l+1)(2L+1)]^{1/2}}\int G_p(r,r')\frac{r_<^l}{r_>^{l+1}}\delta n_L(r')(r')^2dr'\right]Y_L^0(\hat{\mathbf{r}}) , \tag{A8}$$

where we have shown that the integral over Ω is zero for $k \neq 0$, and we introduced the coefficient

$$c(p,l,L)=\int Y_p^0(\Omega)Y_l^0(\Omega)Y_L^0(\Omega)d\Omega \ . \tag{A9}$$

We show now that the second term on the right-hand side of Eq. (A2) is zero. We first express the functional derivative of G^{WDA} as

$$\frac{\delta G^{\mathrm{WDA}}(|\mathbf{r}-\mathbf{r}'|;\bar{n}(\mathbf{r}))}{\delta n(\mathbf{r}'')}=\frac{\partial G^{\mathrm{WDA}}(|\mathbf{r}-\mathbf{r}'|;\bar{n}(\mathbf{r}))}{\partial \bar{n}(\mathbf{r})}\frac{\delta \bar{n}(\mathbf{r})}{\delta n(\mathbf{r}'')} \tag{A10}$$

and, using the functional derivative of the sum rule Eq. (7), we have

$$\frac{\delta \bar{n}(\mathbf{r})}{\delta n(\mathbf{r}'')}=-\frac{G^{\mathrm{WDA}}(|\mathbf{r}-\mathbf{r}''|;\bar{n}(\mathbf{r}))}{\xi(\mathbf{r})} \tag{A11}$$

with

$$\xi(\mathbf{r})=\int \frac{\partial G(|\mathbf{r}-\mathbf{r}_1|;\bar{n}(\mathbf{r}))}{\partial \bar{n}(\mathbf{r})}n(\mathbf{r}_1)d\mathbf{r}_1 \ . \tag{A12}$$

The partial derivative of G^{WDA} in Eq. (A10) and the function $\xi(\mathbf{r})$ are $\mathbf{r}''$ independent [$\xi(\mathbf{r})$ depends only on the radial distance r]; consequently the integral over $\mathbf{r}''$ of the second term in Eq. (A2) reduces to

$$\int G^{\mathrm{WDA}}(|\mathbf{r}-\mathbf{r}''|;\bar{n}(\mathbf{r}))\delta n(\mathbf{r}'')d\mathbf{r}'' \ ,$$

which is zero as long as Eq. (7) must be verified also for the perturbed system with density $n(\mathbf{r})+\delta n(\mathbf{r})$. This conclusion rests on the approximation that the XC energy functional, $E_{\mathrm{XC}}[n]$, does not depend on the excitation energy.

This result together with Eq. (A8) leads to

$$\delta V_1^{\mathrm{WDA}}(\mathbf{r})=\delta V_{1,L}^{\mathrm{WDA}}(r)Y_L^0(\hat{\mathbf{r}}) \tag{A13}$$

with

$$\delta V_{1,L}^{\mathrm{WDA}}(r)=\tfrac{1}{2}\sum_{p,l}\frac{4\pi c(p,l,L)}{[(2l+1)(2L+1)]^{1/2}} \times \int G_p(r,r')\frac{r_<^l}{r_>^{l+1}}\delta n_L(r')(r')^2dr' \ . \tag{A14}$$

In a similar way we obtain for $\delta V_{2,L}^{\mathrm{WDA}}(r)$

$$\delta V_{2,L}^{\mathrm{WDA}}(r)=\tfrac{1}{2}\sum_{p,l}\frac{4\pi c(p,l,L)}{[(2l+1)(2L+1)]^{1/2}} \times \int G_p(r',r)\frac{r_<^l}{r_>^{l+1}}\delta n_L(r')(r')^2dr' \ . \tag{A15}$$

It remains to obtain $\delta V_{3,L}^{\mathrm{WDA}}(r)$. Let us denote the first and second terms on the right-hand side of Eq. (A4) as $\delta V_3^{\mathrm{WDA},1}(\mathbf{r})$ and $\delta V_3^{\mathrm{WDA},2}(\mathbf{r})$, respectively. To simplify the notation we will use the symbols $(\cdot)$, $(\cdot\cdot)$, and $(\cdot\cdot\cdot)$ for the arguments $(|\mathbf{r}'-\mathbf{r}''|;\bar{n}(\mathbf{r}'))$, $(|\mathbf{r}'-\mathbf{r}|;\bar{n}(\mathbf{r}'))$, and $(|\mathbf{r}'-\mathbf{r}_1|;\bar{n}(\mathbf{r}'))$ of the respective G^{WDA} functions, unless explicitly indicated. We also eliminate the superscript WDA. Thus, for example, $G(\cdot)$ denotes $G^{\mathrm{WDA}}(|\mathbf{r}'-\mathbf{r}''|;\bar{n}(\mathbf{r}'))$. Using Eqs. (A5)–(A7), (A10), and (A11), and the expansion

$$\frac{\partial G(\cdot)}{\partial \bar{n}(\mathbf{r}')}=\sum_p\left[\frac{\partial G(\cdot)}{\partial \bar{n}(\mathbf{r}')}\right]_p Y_p^0(\Omega') \ , \tag{A16}$$

where Ω' stands for the angle between $\mathbf{r}'$ and $\mathbf{r}''$, we obtain after an algebra similar to that of $\delta V_1^{\mathrm{WDA}}(\mathbf{r})$,

$$\delta V_3^{\mathrm{WDA},1}(\mathbf{r})=\left[-\left[\frac{4\pi}{2L+1}\right]^{1/2} \times \int \frac{\varphi(r')}{\xi(r')}G_L(r,r')(r')^2dr'\right]Y_L^0(\hat{\mathbf{r}}) \ , \tag{A17}$$

where

$$\varphi(r')=\sum_{p,l}\frac{4\pi c(plL)}{[(2l+1)(2L+1)]^{1/2}} \times \int \left[\frac{\partial G(\cdot)}{\partial \bar{n}(\mathbf{r}')}\right]_p \frac{r_<^l}{r_>^{l+1}}\delta n_L(r'')(r'')^2dr'' \tag{A18}$$

and $r_>$ and $r_<$ are the greater or the lesser of r' and r''.

It remains to prove that $\delta V_3^{\mathrm{WDA},2}(\mathbf{r})$ also has the angular dependence $Y_L^0(\hat{\mathbf{r}})$. To this end, we first obtain the second functional derivative of the pair-correlation function. From Eqs. (A10)–(A12) we have

$$\frac{\delta^2 G(\cdot)}{\delta n(\mathbf{r})\delta n(\mathbf{r}_1)}=\frac{\partial G(\cdot)}{\partial \bar{n}(\mathbf{r}')}\frac{\delta^2 \bar{n}(\mathbf{r}')}{\delta n(\mathbf{r})\delta n(\mathbf{r}_1)} + \frac{\partial^2 G(\cdot)}{\partial \bar{n}(\mathbf{r}')^2}\frac{\delta \bar{n}(\mathbf{r}')}{\delta n(\mathbf{r})}\frac{\delta \bar{n}(\mathbf{r}')}{\delta n(\mathbf{r}_1)} \tag{A19}$$

and

$$\frac{\delta^2 \bar{n}(\mathbf{r}')}{\delta n(\mathbf{r})\delta n(\mathbf{r}_1)}=-\frac{1}{\xi(r')}\frac{\partial G(\cdot\cdot)}{\partial n(\mathbf{r}')}\frac{\delta \bar{n}(\mathbf{r}')}{\delta n(\mathbf{r}_1)}+\frac{G(\cdot\cdot)}{\xi^2(r')}\left[\frac{\partial G(\cdot\cdot\cdot)}{\partial \bar{n}(\mathbf{r}')}+\int \frac{\delta}{\delta n(\mathbf{r}_1)}\left[\frac{\partial G(\cdot\cdot)}{\partial \bar{n}(\mathbf{r}')}\right]n(\mathbf{r})d\mathbf{r}\right] \ . \tag{A20}$$

The integral in the second term of Eq. (A20) is zero because of Eq. (7):

$$\int \frac{\delta}{\delta n(\mathbf{r}_1)}\left[\frac{\partial G(\cdot\cdot)}{\partial \bar{n}(\mathbf{r}')}\right] n(\mathbf{r})d\mathbf{r} = -\frac{G(\cdots)}{\xi(r')}\int \frac{\partial^2 G(\cdot\cdot)}{\partial \bar{n}(\mathbf{r}')^2} n(\mathbf{r})d\mathbf{r}$$
$$= -\frac{G(\cdots)}{\xi(r')^2}\frac{\partial}{\partial \bar{n}(\mathbf{r}')^2}\int G(|\mathbf{r}'-\mathbf{r}|;\bar{n}(\mathbf{r}'))n(\mathbf{r})d\mathbf{r}$$
$$=0 . \tag{A21}$$

Then Eq. (A19) reads

$$\frac{\delta^2 G(\cdot)}{\delta n(\mathbf{r})\delta n(\mathbf{r}')} = \frac{1}{\xi(r')^2}\left[\frac{\partial G(\cdot)}{\partial \bar{n}(\mathbf{r}')}\left[G(\cdots)\frac{\partial G(\cdot\cdot)}{\partial \bar{n}(\mathbf{r}')} + G(\cdot\cdot)\frac{\partial G(\cdots)}{\partial \bar{n}(\mathbf{r}')}\right] + G(\cdot\cdot)G(\cdots)\frac{\partial^2 G(\cdot)}{\partial \bar{n}(\mathbf{r}')^2}\right] . \tag{A22}$$

The angular dependence is the same for both terms on the right-hand side of Eq. (A22) because they differ only in the partial derivatives with respect to $\bar{n}$, which does not introduce additional angular terms. The integral in $\mathbf{r}_1$ of $\delta V_3^{\mathrm{WDA},2}(\mathbf{r})$ can be expressed, after angular integration, as

$$\int \frac{\delta^2 G(\cdot)}{\delta n(\mathbf{r})\delta n(\mathbf{r}_1)}\delta n_L(r_1)Y_L^0(\hat{\mathbf{r}}_1)d\mathbf{r}_1 = \frac{G(\cdot\cdot)}{\xi(r')^2}\left[\left[\frac{\partial f_L(r')}{\partial \bar{n}(r')} + f_L(r')\frac{\partial}{\partial \bar{n}(\mathbf{r}')}\ln G(\cdot\cdot)\right]\frac{\partial G(\cdot)}{\partial \bar{n}(\mathbf{r}')} + \frac{\partial^2 G(\cdot)}{\partial \bar{n}(\mathbf{r}')^2}f_L(r')\right] Y_L^0(\hat{\mathbf{r}}') , \tag{A23}$$

where

$$f_L(r') = \left[\frac{4\pi}{2L+1}\right]^{1/2}\int dr_1\, r_1^2 G_L(r',r_1)\delta n_L(r_1) . \tag{A24}$$

After angular integration we obtain

$$\delta V_3^{\mathrm{WDA},2}(\mathbf{r}) = \left[\frac{1}{2}\left[\frac{4\pi}{2L+1}\right]^{1/2}\int dr'(r')^2\frac{\chi_L(r')}{\xi^2(r')}G_L(r',r)n(r')\right] Y_L^0(\hat{\mathbf{r}}) , \tag{A25}$$

where

$$\chi_L(r') = \sum_{p,l}\frac{4\pi C(p,l,L)}{[(2l+1)(2L+1)]^{1/2}}\int dr''(r')^2\frac{r_<^l}{r_>^l}n(r'')\left[\left[\frac{\partial f_L(r')}{\partial \bar{n}(r')} + f_L(r')\frac{\partial}{\partial \bar{n}(r')}\ln G_L(r',r)\right]\left[\frac{\partial G(\cdot)}{\partial \bar{n}(\mathbf{r}')}\right]_p + f_L(r')\left[\frac{\partial^2 G(\cdot)}{\partial \bar{n}(r')^2}\right]_p\right] . \tag{A26}$$

From Eqs. (A17) and (A25) we finally obtain

$$\delta V_{3,L}^{\mathrm{WDA}}(r) = \left[\frac{4\pi}{2L+1}\right]^{1/2}\left[\int dr'(r')^2\frac{G_L(r,r')}{\xi(r')}n(r')\left[-\varphi(r') + \frac{1}{2}\frac{\chi_L(r')}{\xi(r')}\right]\right] . \tag{A27}$$

APPENDIX B: NUMERICAL PROCEDURES

Introducing the differential operator

$$K^{nll_1} \equiv -\frac{1}{2}\frac{d^2}{dr^2} + \frac{l_1(l_1+1)}{2r^2} + V_{\mathrm{eff}}(r) - \varepsilon_{nl} \tag{B1}$$

the radial Sternheimer Eq. (37) reads

$$K^{nll_1}v_{l_1,L}^{nl}(r) = -\delta V_{\mathrm{eff},L}(r)u_{nl}(r) \tag{B2}$$

or, after discretizing,

$$\sum_j K_{ij}^{nll_1}V_{l_1,L}^{nl}(r_j) = -\delta V_{\mathrm{eff},L}(r_i)u_{nl}(r_i) . \tag{B3}$$

It can be shown that for given L and l the only nonzero $A(L,l,l_1)$ values in Eq. (39) are reached when $l_1 = |L-l|, |L-l|+2, |L-l|+4, \ldots, L+l$. For even L, one of the l_1 values should be $l_1 = l$, leading to a noninvertible K_{ij}^{nll} matrix. For odd L, Eq. (B3) can be inverted, giving

$$v_{l_1,L}^{nl}(r_i) = -\sum_j\left[K_{ij}^{nll_1}\right]^{-1}\delta V_{\mathrm{eff},L}(r_j)u_{nl}(r_j) . \tag{B4}$$

Substituting Eq. (B4) into Eq. (40), the discretized induced density reads

$$\delta n_L(r_i) = -\sum_j m_{ij}\delta V_{\mathrm{eff},L}(r_j) , \tag{B5}$$

where

$$m_{ij} = 4\sum_{n,l,l_1}\frac{u_{nl}(r_i)u_{nl}(r_j)}{r_i^2}A(L,l,l_1)(K_{ij}^{nll_1})^{-1} . \tag{B6}$$

The discretized induced potential can be written as

$$\delta V_{\mathrm{eff},L}(r_j)=r_j^L+\sum_k t_{jk}\delta n_L(r_k)\ , \tag{B7}$$

where in the case of LDA we have

$$t_{jk}^{\mathrm{LDA}}=\frac{4\pi}{2L+1}\omega_k r_k^2\frac{r_<^L}{r_>^{l+1}}+\frac{\partial^2}{\partial n^2}(n\varepsilon_{\mathrm{XC}})_j\delta_{jk} \tag{B8}$$

and in the case of the WDA we have

$$t_{jk}^{\mathrm{WDA}}=\left[\frac{4\pi}{2L+1}\frac{r_<^L}{r_>^{L+1}}+\left[\frac{\delta^2 E_{\mathrm{XC}}^{\mathrm{WDA}}}{\delta n(r_j)\delta n(r_k)}\right]_L\right]\omega_k r_k^2 \tag{B9}$$

with ω_k being the numerical integration weight for the point r_k. The radial component $[\delta^2 E_{\mathrm{XC}}/\delta n(r)\delta n(r')]_L$ has been defined in Appendix A [see also Eq. (26)]. Now, Eq. (B5) can be written as

$$\delta n_L(r_i)=-\sum_j m_{ij}\left[r_j^L+\sum_k t_{jk}\delta n_L(r_k)\right] \tag{B10}$$

or, in compact matrix form,

$$(\underline{1}+\underline{\mathbf{M}}\,\underline{\mathbf{T}})\overline{\delta n_L}=-\underline{\mathbf{M}}\mathbf{r}^L\ , \tag{B11}$$

where $\mathbf{r}$ and $\overline{\delta n_L}$ are column vectors with components $(r_1,r_2,\ldots,r_n)$ and $[\delta n_L(r_1),(\delta n_L(r_2),\ldots,(\delta n_L(r_n)]$, respectively, and n is the number of points in the integration mesh.

The boundary conditions that we impose to solve Eq. (B11) are $\delta n(0)=0$ and $\delta n(r_{n+1})=0$, because $v_{l_1}^{nl}(r)\approx r^{l_1+1}$ as $r\approx 0$ [see Eq. (37)] and $v_{l_1}^{nl}(r)\approx u_{nl}(r)$ as $r\approx\infty$. The matrix K_{ij} is tridiagonal because we have used three-point formulas for the r derivatives. The number of points in the integration mesh is optimized to fulfill Sorbello's force sum rule. We have also checked the stability of our results using a five-points formula for the second derivative in the K_{ij} operator.

*Present address: Departament d'Estructura i Constituents de la Matéria, Facultat de Física, Universitat de Barcelona, E-08028 Barcelona, Spain.

[1]W. D. Knight, K. Clemenger, W. A. de Heer, and W. A. Saunders, Phys. Rev. B **31**, 2539 (1985).
[2]W. A. de Heer, K. Selby, V. Kresin, J. Masui, M. Vollmer, A. Châtelain, and W. D. Knight, Phys. Rev. Lett. **59**, 1805 (1987).
[3]K. Selby, M. Vollmer, J. Masui, V. Kresin, W. A. de Heer, and W. D. Knight, Z. Phys. D **12**, 477 (1989).
[4]K. Selby, M. Vollmer, J. Masui, V. Kresin, W. A. de Heer, and W. D. Knight, Phys. Rev. B **40**, 5417 (1989).
[5]C. Bréchignac, Ph. Cahuzac, F. Carlier, and J. Leygnier, Chem. Phys. Lett. **164**, 433 (1989).
[6]J. H. Parks and S. A. McDonald, Phys. Rev. Lett. **62**, 2301 (1989).
[7]G. Mie, Ann. Phys. (Leipzig) [Folge 4] **25**, 377 (1908).
[8]For a recent review, see W. A. de Heer, W. D. Knight, M. Y. Chou, and M. L. Cohen, in *Solid State Physics,* edited by H. Ehrenreich and D. Turnbull (Academic, Nwe York, 1987), Vol. 40, p. 93.
[9]P. Hohenberg and W. Kohn, Phys. Rev. **136**, B864 (1964).
[10]W. Kohn and L. J. Sham, Phys. Rev. **140**, A1133 (1965).
[11]A. Zangwill and P. Soven, Phys. Rev. A **21**, 1561 (1980).
[12]W. Ekardt, Phys. Rev. Lett. **52**, 1925 (1984); Phys. Rev. B **31**, 6360 (1985).
[13]D. E. Beck, Phys. Rev. B **35**, 7325 (1987).
[14]D. E. Beck, Phys. Rev. B **30**, 6935 (1984).
[15]Ll. Serra, F. Garcías, M. Barranco, J. Navarro, L. C. Balbás, and A. Mañanes, Phys. Rev. B **39**, 8247 (1989).
[16]Ll. Serra, F. Garcías, M. Barranco, J. Navarro, L. C. Balbás, A. Rubio, and A. Mañanes, J. Phys. Condens. Matter **1**, 10 391 (1989).
[17]G. Bertsh and W. Ekardt, Phys. Rev. B **32**, 7659 (1985).
[18]P. Stampfly and K. H. Bennemann, Phys. Rev. A **39**, 1007 (1989).
[19]J. P. Perdew and A. Zunger, Phys. Rev. B **23**, 5048 (1981).
[20]J. A. Alonso and L. A. Girifalco, Phys. Rev. B **17**, 3735 (1978).
[21]O. Gunnarson, M. Jonson, and B. I. Lundqvist, Phys. Rev. B **20**, 3136 (1979).
[22]H. Przybylski and G. Borstel, Solid State Commun. **49**, 317 (1984); **52**, 713 (1984).
[23]L. C. Balbás, A. Rubio, J. A. Alonso, and G. Borstel, J. Chim. Phys. **86**, 799 (1989).
[24]M. P. Iñiguez, J. A. Alonso, A. Rubio, M. J. López, and L. C. Balbás, Phys. Rev. B **41**, 5595 (1990).
[25]*The Inhomogeneous Electron Gas,* edited by N. H. March and B. I. Lundqvist (Plenum, New York, 1983).
[26]E. Chacon and P. Tarazona, Phys. Rev. B **37**, 4013 (1988).
[27]G. D. Mahan, Phys. Rev. A **22**, 1780 (1980).
[28]Ll. Serra, F. Garcias, M. Barranco, N. Barberan, and J. Navarro, Phys. Rev. B **41**, 3434 (1990).
[29]Z. Y. Zhang, D. C. Langreth, and J. P. Perdew, Phys. Rev. B **41**, 5674 (1990).
[30]E. Krotscheck, W. Kohn, and G. X. Qian, Phys. Rev. B **32**, 5693 (1985).
[31]L. C. Balbás, J. A. Alonso, and G. Borstel, Z. Phys. D **6**, 219 (1987).
[32]L. C. Balbás, A. Rubio, J. A. Alonso, and G. Borstel, Chem. Phys. **120**, 239 (1988).
[33]A. Rubio, L. C. Balbás, and J. A. Alonso (unpublished work).
[34]S. Saito, S. B. Zhang, S. G. Louie, and M. L. Cohen, Phys. Rev. B **40**, 3643 (1989).
[35]E. Chacon (private communication).
[36]R. S. Sorbello, Solid State Commun. **48**, 989 (1983).
[37]N. D. Lang and W. Kohn, Phys. Rev. B **7**, 3541 (1973).
[38]D. R. Snider and R. S. Sorbello, Phys. Rev. B **28**, 5702 (1983).
[39]D. C. Langreth and M. J. Mehl, Phys. Rev. B **28**, 1809 (1983); **29**, 2310 (1984).
[40]S. Ossicini, C. M. Bertoni, and P. Gies, Europhys. Lett. **1**, 661 (1986).
[41]J. L. Martins, R. Car, and J. Buttet, Surf. Sci. **106**, 265 (1981).
[42]A. Rubio, L. C. Balbás, and J. A. Alonso, Solid State Commun. **75**, 139 (1990).
[43]W. A. de Heer, P. Milani, and A. Châtelain, Phys. Rev. Lett. **63**, 2843 (1989).
[44]M. J. López, Doctoral dissertation, Universidad de Valladolid, 1990 (unpublished).
[45]A. A. Lushnikov, V. V. Maksimenko, and A. J. Simonov, in *Electromagnetic Surface Modes,* edited by A. D. Boardman (Wiley, New York, 1982).